3D Quantitative microwave imaging from sparsely measured data with Huber regularization

Funing Bai and Aleksandra Pižurica

Department of Telecommunications and Information Processing (IPI-TELIN-Iminds),
Ghent University, St-Pietersnieuwstraat 41, B-9000 Gent, Belgium

ABSTRACT

Reconstructing complex permittivity profiles of dielectric objects from measurements of the microwave scattered field is a non-linear ill posed inverse problem. We analyze the performance of the Huber regularizer in the application, studying the influence of the parameters under different noise levels. Moreover, we evaluate the whole approach on real 3D electromagnetic measurements. Our focus is on reconstructions from relatively few measurements (sparse measurements) to speed up the reconstruction process.

Keywords: inverse problem, microwave imaging, Huber function, sparsity, real electromagnetic measurements.

1. INTRODUCTION

Quantitative microwave imaging aims at reconstructing the exact permittivity profile of an unknown scattering object by illuminating the object with microwaves and by measuring the scattered field. Different regularization approaches have been proposed for solving this nonlinear ill-posed inverse problem.[1–5] Multiplicative smoothing (MS)[1] applies Tikhonov regularization in a multiplicative fashion and hence it tends to oversmooth the results, while Value Picking (VP)[2] produces sharp results but is applicable only to piece-wise constant profiles with few distinct permittivities values. An edge preserving regularization[3] was imposed on the real and imaginary part of the complex permittivity separately. Total variation (TV) was used as a multiplicative constraint[4] and a Line Process model was employed by Caorsi *et al.*[5]

We introduced previously a new regularization approach based on the Huber function,[6] which is suitable not only for piecewise constant profiles, but also for more general permittivity profiles (that are of interest e.g. in biomedical imaging).[7] We demonstrated already very encouraging first results on simulated data.[6] In this paper, we perform an analysis of this regularizer, studying the influence of the parameters under different levels of noise. Moreover, we evaluate the whole approach not only on simulated data but also on real 3D electromagnetic measurements. Our focus is on reconstructions from relatively few measurements (sparse measurements), which are of interest to speed up the reconstruction process.

We consider in this paper scattering measurements of 3D targets from the Institute Fresnel, that are available in the so-called Fresnel database, and that are commonly used to test new algorithms in the inverse scattering community. A special issue of Inverse Problems[8] was devoted to reconstructions on these benchmark experimental data in order to enable fair comparison of the current and future methods using the same measurements. Moreover, validating inversion algorithms on experimental data is much more reliable than using simulations only, which are prone to inverse crime.[9] Reconstructions from the experimental data are quite challenging due to measurement noise and discretization noise as well as mismatch between the actual incident fields and their simulation in the forward solvers. Furthermore, it is interesting to explore potentials for speeding up the reconstruction process. In quantitative microwave imaging, using a smaller number of data points (i.e. performing a sparse reconstruction), is especially of interest because long computation times are currently limiting practical

Further author information: (Send correspondence to Funing Bai)
Funing Bai: E-mail: Funing.Bai@telin.ugent.be, Telephone: +32 9 264 8905
Aleksandra Pižurica: E-mail: Aleksandra.Pizurica@telin.ugent.be, Telephone: +32 9 264 3415

use of this imaging modality. We show that using our approach reconstruction times for 3D objects can be drastically reduced (e.g., from several hours to several minutes on the same computer architecure, without affecting significantly the quality of the reconstructed results).

Our results on experimental data from the 3D Fresnel database motivate strongly the use of Huber regularization. The advantages over related regularization methods, like MS and VP that were demonstrated previously on simulated data are now confirmed with real experimental data. Moreover, analysis of the influence of different parameters presented in this paper gives new insights in the behavior of the Huber regularizer in quantitative microwave imaging and provides useful guidelines for its practical use in different scenarios (e.g. different levels of measurement noise). This paper is organized as follows. In Section 2 the electromagnetic inverse scattering problem and Gauss-Newton method are revisited. The Huber function is discussed in Section 3 and experimental validations are presented in Section 4. Section 5 concludes the paper.

2. PROBLEM FORMULATION

We start from a classical problem formulation in quantitative microwave tomography.[1,2] As in our earlier work,[6] the unknown permittivity of a reconstruction domain $\mathcal{D}$ is discretized in N^ε reconstruction variables $\boldsymbol{\varepsilon} = [\varepsilon_1, \cdots, \varepsilon_\nu, \cdots, \varepsilon_{N^\varepsilon}]$. In order to reconstruct the permittivity profile $\boldsymbol{\varepsilon}$, an iterative method is used on a grid with these N^ε cube cells, alternating between the forward and the inverse problem. In each step of the iterative method, simulated scattered fields $\mathbf{e}^{scat}(\boldsymbol{\varepsilon})$ are compared with the measured fields $\mathbf{e}^{meas}$ and the permittivity profile is updated based on this difference. This inverse problem is solved by minimizing a cost function

$$F(\boldsymbol{\varepsilon}) = F^{LS}(\boldsymbol{\varepsilon}) + \mu F^R(\boldsymbol{\varepsilon}) \tag{1}$$

where $F^R(\boldsymbol{\varepsilon})$ is a regularization function, $\mu \geq 0$ is a regularization parameter and $F^{LS}(\boldsymbol{\varepsilon})$ is the least squares data fit:

$$F^{LS}(\boldsymbol{\varepsilon}) = \frac{\|\mathbf{e}^{meas} - \mathbf{e}^{scat}(\boldsymbol{\varepsilon})\|^2}{\|\mathbf{e}^{meas}\|^2} \tag{2}$$

$\mathbf{e}^{meas}$ and $\mathbf{e}^{scat}(\boldsymbol{\varepsilon})$ are N^d-dimensional vectors that represent the measured and the simulated scattered fields, respectively. We define the regularization function $F^R(\boldsymbol{\varepsilon})$ as

$$F^R(\boldsymbol{\varepsilon}) = \frac{1}{2} \sum_\nu \sum_{\nu' \in N_\nu} g_\gamma(\varepsilon_\nu - \varepsilon_{\nu'}) \tag{3}$$

where g_γ is a potential function with parameter γ and ν' denotes a spatial position neighboring ν in the neighborhood system N_ν. We use 8 neighbors in 2D and 26 neighbors in 3D as a compromise between reconstruction quality and complexity.

As in our earlier work,[6] we consider minimization by an approximate line search along a modified Gauss-Newton descent direction, which requires a positive definite Gauss-Newton Hessian matrix. The complex permittivity in iteration k is updated as $\boldsymbol{\varepsilon}_{k+1} = \boldsymbol{\varepsilon}_k + \beta_k \boldsymbol{\Delta\varepsilon}_k$. β_k is calculated from the line search[2] and $\boldsymbol{\Delta\varepsilon}_k$ is obtained from

$$(\mathbf{J}_k^H \mathbf{J}_k + \lambda^2 \boldsymbol{\Sigma}_k^R) \boldsymbol{\Delta\varepsilon}_k = -(\mathbf{J}_k^H [\mathbf{e}^{scat}(\boldsymbol{\varepsilon}_k) - \mathbf{e}^{meas}] + \lambda^2 \boldsymbol{\Omega}_k^{R*}) \tag{4}$$

where $(.)^H$ stands for Hermitian transpose and $(.)^*$ denotes the complex conjugate. In the following, the subscript k is omitted for compactness. The factor $\mathbf{J}^H\mathbf{J} + \lambda^2 \boldsymbol{\Sigma}^R$ is known as a Gauss-Newton Hessian matrix. The trade-off parameter λ is given by $\lambda^2 = \mu \|\mathbf{e}^{meas}\|^2$.[2] $\mathbf{J}$ is the $N^d \times N^\varepsilon$ Jacobian matrix, which contains the derivatives of the scattered field components with respect to the optimization variables: $J_{d,\nu} = \partial e_d^{scat} / \partial \varepsilon_\nu$; $\boldsymbol{\Omega}^{R*}$ is an $N^\varepsilon-$dimensional vector that contains the derivatives of the regularizing function, $\Omega_\nu^{R*} = \partial F^R / \partial \varepsilon_\nu^*$; $\boldsymbol{\Sigma}^R$ is a $N^\varepsilon \times N^\varepsilon$ matrix $\Sigma_{\nu,\nu'}^R = \partial^2 F^R / \partial \varepsilon_{\nu'} \partial \varepsilon_\nu^*$. We addressed this problem in a previous work,[6] by deriving $\boldsymbol{\Omega}^{R*}$ and $\boldsymbol{\Sigma}^R$ for the Huber function. In this paper, we will validate this framework on real data.

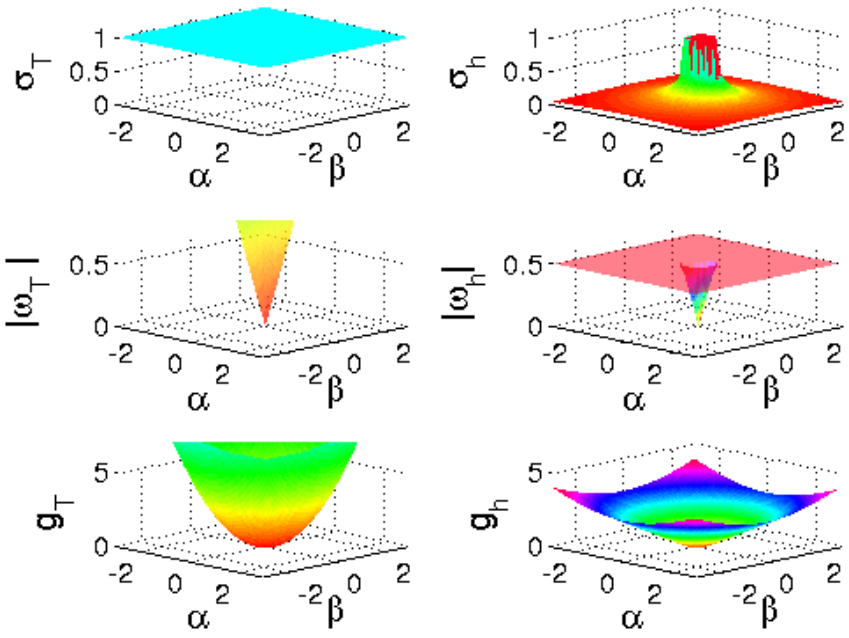

Figure 1. The qualitative shape of the Huber (right) and Tikhonov (left) functions in the complex domain.

3. HUBER REGULARIZATION

Let $\eta = \alpha + j\beta$ denote a complex number, being a difference between two neighboring complex permittivities: $\eta = \varepsilon_\nu - \varepsilon_{\nu'}$. In this paper, we will illustrate the performance of the Huber function acting as the potential function g_γ in the regularization term of (3). The model

$$g_h(\eta) = \begin{cases} |\eta|^2 & |\eta| \le \gamma \\ 2\gamma|\eta| - \gamma^2 & otherwise \end{cases} \tag{5}$$

can be considered as a 2D extension of the 1D Huber model $g_h(r)$.[10] In our earlier work,[6] we demonstrated the potential of the Huber regularization (5) in quantitative microwave imaging, but on simulated data only and without studying the behavior of the parameter γ of this model.

For the chosen regularization function g_γ in (3), we derive $\mathbf{\Omega}^{R*}$ and $\mathbf{\Sigma}^R$ in (4). Taking into account that $|\eta|^2 = \eta\eta^*$, it can be shown that for the Huber function from (5)

$$\begin{aligned} \Omega_\nu^{R*} &= \frac{\partial F^R}{\partial \varepsilon_\nu^*} \\ &= \sum_{\nu' \in N_\nu} \begin{cases} (\varepsilon_\nu - \varepsilon_{\nu'}) & |\varepsilon_\nu - \varepsilon_{\nu'}| \le \gamma \\ \gamma \dfrac{(\varepsilon_\nu - \varepsilon_{\nu'})}{|\varepsilon_\nu - \varepsilon_{\nu'}|} & otherwise \end{cases} \end{aligned} \tag{6}$$

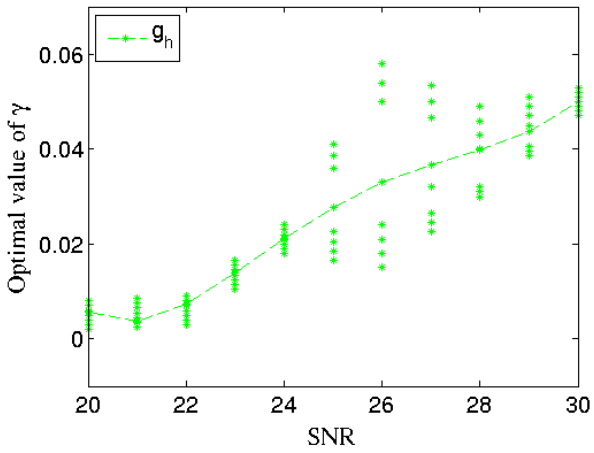

Figure 2. Optimal values of gamma (yielding the smallest reconstruction errors) as a function of the SNR for g_h.

We obtain the diagonal elements of $\mathbf{\Sigma}^R$ as

$$\begin{aligned} \Sigma^R_{\nu,\nu} &= \frac{\partial^2 F^R}{\partial \varepsilon_\nu \partial \varepsilon^*_\nu} \\ &= \sum_{\nu' \in N_\nu} \begin{cases} 1 & |\varepsilon_\nu - \varepsilon_{\nu'}| \le \gamma \\ \dfrac{\gamma}{2|\varepsilon_\nu - \varepsilon_{\nu'}|} & otherwise \end{cases} \end{aligned} \tag{7}$$

and the non-diagonal elements as

$$\begin{aligned} \Sigma^R_{\nu,\nu'} &= \frac{\partial^2 F^R}{\partial \varepsilon_{\nu'} \partial \varepsilon^*_\nu} \\ &= \begin{cases} -1 & |\varepsilon_\nu - \varepsilon_{\nu'}| \le \gamma \\ -\dfrac{\gamma}{2|\varepsilon_\nu - \varepsilon_{\nu'}|} & otherwise \end{cases} \end{aligned} \tag{8}$$

Fig. 1 illustrates the Huber function $g_h(\eta)$ and the Tikhonov function $g_T(\eta)$ in the complex domain ($\eta = \alpha + j\beta$), together with the corresponding magnitude $|\omega(\eta)|$ and $\sigma(\eta)$ functions. Note that $|\omega|$, which is an indication of the smoothing strength, increases monotonically with $|\eta|$ in the whole domain of $|\omega_T|$, whereas $|\omega_h|$ only does so in the smoothing interval $|\eta| < \gamma$ and remains a constant, allowing limited (bounded) smoothing, outside this interval. The interaction σ, which determines the interaction between neighboring pixels also behaves differently for the two regularizations: σ_h is smaller for large $|\eta|$ and approaches 0 as $|\eta|$ goes to ∞, while σ_T holds the same interaction power in the whole domain. This way, the Huber function preserves edges and reduces the effect of outliers. A pseudo-code of the reconstruction algorithm is given in our earlier work.[6]

To analyze the behavior of the Huber function in quantitative microwave imaging when minimizing (4) with the Gauss-Newton method and to optimize its parameter γ for the reconstruction of piece-wise constant objects at different noise levels, we experiment with different levels of additive white Gaussian noise resulting in signal-to-noise (SNR) from 20dB to 30dB. To evaluate the quality of the permittivity reconstructions, the reconstruction error R is defined as

$$R = \frac{\| \boldsymbol{\varepsilon}^{rec} - \boldsymbol{\varepsilon}^{ref} \|^2}{\|\boldsymbol{\varepsilon}^{ref}\|^2} \tag{9}$$

which expresses the normalized squared difference between the reference $\boldsymbol{\varepsilon}^{ref}$ and reconstructed $\boldsymbol{\varepsilon}^{rec}$ permittivity values on the grid.

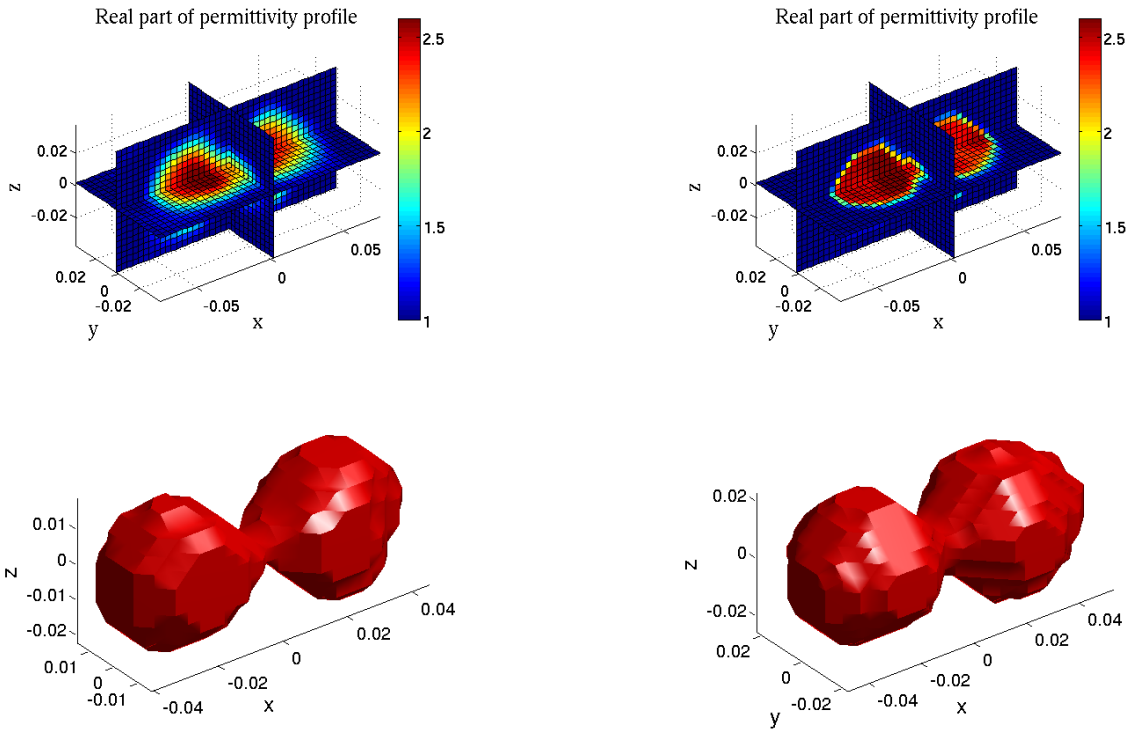

(a) MS (b) g_h

Figure 3. Real part of the complex permittivity and a 3D view (cut value = 2.2) of the surface for the *Two Spheres* target. Reconstructions (using 243 data) from the sparsest antenna configuration at 4GHz with: (a) MS, (b) g_h.

In Fig. 2, we show that the optimal value of γ is increasing when the SNR increases. Keep in mind that this optimal value is only from the reconstruction error point of view, which does not mean it will yield sharpest edges. The plot in Fig. 2 also shows that $\gamma \approx 0.008$ is a good choice for SNR = 20 dB, which can be considered[1] as the noise level for the experimental data in Section 4. For the 26 neighborhood system, the reconstruction results are not very sensitive to γ, so we can use the same parameter for different targets at a certain noise level.

4. 3D EXPERIMENTAL DATA VALIDATION

To test the effectiveness of our inversion algorithms in even more challenging 3D real data, we select 3D targets: Two Spheres, Two Cubes and Cube of Spheres from the Fresnel database with antenna configuration described by Geffrin and Sabouroux.[11] These carefully measured experimental data have been inverted with various methods by several authors.[12] In our experiments, for each target, Multiplicative Smoothing (MS)[2] and Huber estimation are employed in independent reconstructions and the results are compared. In our experiments, BICGSTAB-FFT (biconjugate gradient stabilized method-Fast Fourier Transform) forward solver is used to accelerate the calculations.

The reconstructions with each of the analyzed methods were run on a six-core Intel i7 980x processor (3.33GHz) with 24GByte memory (threads = 8). With full dataset, the reconstruction time is 3 hours. Using sparse data and the same hardware parameters, the reconstruction takes 30 minutes in 10 iterations or with a stop criterion $F^{LS} = 10^{-3}$.

All reconstructions start from the domain filled with air as an initial estimate of the permittivity. We use the same discretization for both the forward and inverse grids. Only the real parts of the permittivities are shown, since the imaginary parts are negligible. We used $\gamma = 0.008$ for the Huber function and the regularization parameter was set to $\mu = 10^{-4}$. For MS, we used $\mu = 10^{-3}$, as was suggested by the authors.[1]

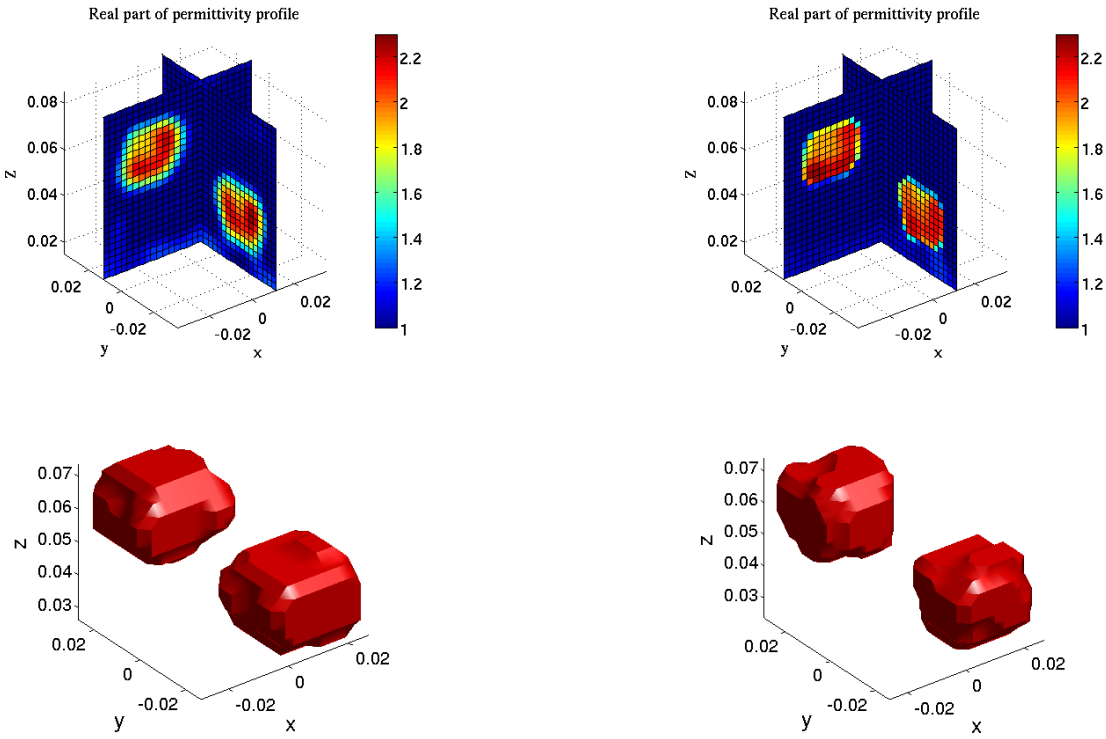

(a) MS (b) g_h

Figure 4. Real part of the complex permittivity and a 3D view (cut value = 1.6) of the surface for *Two Cubes* target. Reconstructions (using 736 data) from the sparse antenna configuration at 8GHz with: (a) MS, (b) g_h.

Two Spheres

This target consists of two dielectric spheres 50 mm in diameter with a permittivity of 2.6. One is centered at the point (-0.025m, 0, 0) the other at (0.025m, 0, 0). We use 41 transmitters and 4 receivers, resulting in a data vector $\mathbf{e}^{meas}$ of length $N^d = 243$. The reconstruction domain in the inverse solver is discretized in $40 \times 20 \times 20$ cube inverse problem cells (16000 permittivity unknowns) with a cell size of 4.0 mm. The reconstructions using MS and Huber regularization are shown in Fig. 3. The reconstruction with MS Fig. 3 (a) oversmoothed the edges as expected. With Huber regularization, see Fig. 3 (b), the shape of two spheres is well reconstructed and the value is very close to the reference value which is $2.6 - j0$. We can also notice better reconstructed 3D surface with Huber regularization compared to MS.

Two Cubes

This target consists of two dielectric cubes with side 25mm and a permittivity of 2.3. One is centered at (0.0125m, -0.0125m, 0.0375m) and the other at (-0.0125m, 0.0125m, 0.0625m). We subsampled the (8GHz) data by 41 transmitters and 12 receivers, yielding a data vector with dimension N^d= 736. The reconstruction domain is discretized in $25 \times 25 \times 25$ cells with a cell size of 2.80 mm ($0.075\lambda_0$), yielding a total of 15625 permittivity unknowns. The reconstructions using MS and Huber regularization are shown in Fig. 4. The results of MS in Fig. 4 (a) shows oversmoothed edges. With Huber regularization, see the result in Fig. 4 (b), the cubes are reconstructed in the right locations but some parts of the edges are a bit eroded.

Cube of Spheres

This target is an aggregate of 27 dielectric spheres in a $3 \times 3 \times 3$ cubic stacking with side 47.6 mm. Each sphere has a diameter of 15.9 mm and a permittivity of 2.6. We subsampled the (8GHz) data by 41 transmitters and 12 receivers, yielding a data vector with dimension $N^d = 736$. The reconstruction domain $\mathcal{D}$ is a 6cm$\times$ 6cm$\times$ 6.9 cm box, centered at the point (0, 0, 0.0145 m) and is discretized in $20 \times 20 \times 23$ cells with cell size 3 mm, yielding

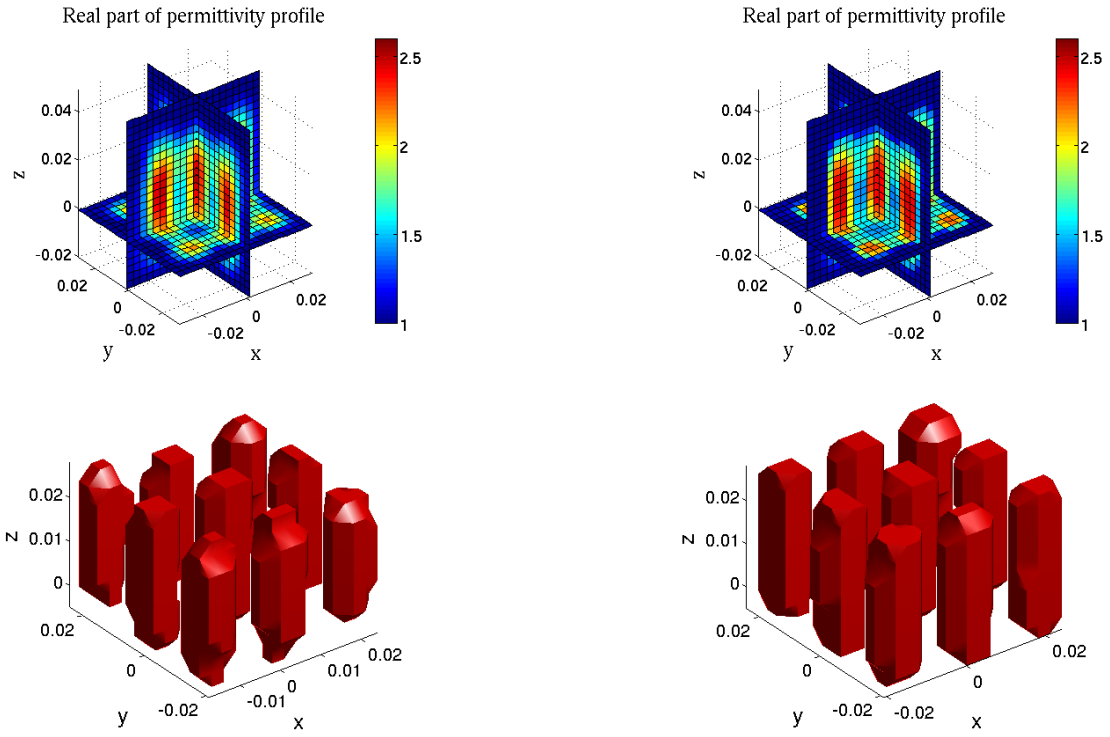

(a) MS (b) g_h

Figure 5. Real part of the complex permittivity and a 3D view (cut value = 2.0) of the surface for *Cube of Spheres* target. Reconstructions (using 736 data) from the sparse antenna configuration at 8GHz with: (a) MS, (b) g_h.

a total of 9200 permittivity unknowns. Fig. 5 shows the results from the different methods. The reconstruction with MS in Fig. 5 (a) eroded the objects in z direction. With Huber regularization (Fig. 5 (b)), the edges are better reconstructed. The three spheres in z direction cannot be distinguished in both cases, and this is because the receiving antennas were placed only in xy plane.

5. SUMMARY

The results on experimental data from the 3D Fresnel database motivate strongly the use of Huber regularization in quantitative microwave tomography. The advantages over related regularization methods, that were demonstrated previously on simulated data are now confirmed with real experimental data. Moreover, the analysis of the influence of different parameters presented in this paper gives new insights in the behavior of the Huber regularizer in quantitative microwave imaging and provides useful guidelines for its practical use in different scenarios (e.g. different levels of measurement noise).

REFERENCES

[1] Zaeytijd, J. D. and Franchois, A., "Three-dimensional quantitative microwave imaging from measured data with multiplicative smoothing and value picking regularization," *Inverse Probl.* **25**(2), 024004 (2009).

[2] De Zaeytijd, J., Franchois, A., and Geffrin, J., "A new value picking regularization strategy - application to the 3-D electromagnetic inverse scattering problem," *IEEE Trans. Antennas Propag.* **57**, 1133 –1149 (Apr. 2009).

[3] Lobel, P., Pichot, C., Blanc-Feraud, L., and Barlaud, M., "Microwave imaging: Reconstructions from experimental data using conjugate gradient and enhancement by edge-preserving regularization," *Int. Journal of Imaging Syst. and Technol.* **8**(4), 337–342 (1997).

[4] Abubakar, A. and Van Den Berg, P., "Total variation as a multiplicative constraint for solving inverse problems," *IEEE Trans. Image Process.* **10**, 1384 –1392 (Sept. 2001).

[5] Caorsi, S., Gragnani, G., Medicina, S., Pastorino, M., and Zunino, G., "Microwave imaging based on a Markov random field model," *IEEE Trans. Antennas Propag.* **42**, 293–303 (Mar. 1994).

[6] Bai, F., Pižurica, A., Van Loocke, S., Franchois, A., De Zutter, D., and Philips, W., "Quantitative microwave tomography from sparse measurements using a robust Huber regularizer," in [*IEEE Int. Conf. Image Processing (ICIP)*], 2073–2076 (2012).

[7] Bai, F., Franchois, A., De Zaeytijd, J., and Pižurica, A., "Three-dimensional quantitative microwave imaging of realistic numerical breast phantoms using Huber regularization," in [*35th Annual International Conference of the IEEE Engineering in Medicine and Biology Society (EMBS)*], 5135–5138 (July 2013).

[8] Belkebir, K. and Saillard, M., "Special section on testing inversion algorithms against experimental data: inhomogeneous targets," *Inverse Problems* **21**(6), S1–S165 (2005).

[9] Colton, D. and Kress, R., [*Inverse Acoustic and Electromagnetic Scattering Theory*], Springer (1992).

[10] Li, S. Z., [*Markov Random Field Modeling in Image Analysis*], Springer (1995).

[11] Geffrin, J. M. and Sabouroux, P., "Continuing with the Fresnel database: experimental setup and improvements in 3D scattering measurements," *Inverse Probl.* **25**(2), 024001 (2009).

[12] Litman, A. and Crocco, L., "Testing inversion algorithms against experimental data: 3D targets," *Inverse Probl.* **25**(2), 020201 (2009).